DOI: 10.1002/adma.200601472

Simultaneously Increasing the Ductility and Strength of Ultra-Fine-Grained Pure Copper**

By *Yong-Hao Zhao*, *John F. Bingert*, *Xiao-Zhou Liao*, *Bao-Zhi Cui*, *Ke Han*, *Alla V. Sergueeva*, *Amiya K. Mukherjee*, *Ruslan Z. Valiev*, *Terence G. Langdon*, and *Yuntian T. Zhu**

Bulk ultra-fine-grained (UFG) materials produced by severe plastic deformation (SPD)[1] usually have high strength but relatively low ductility at ambient temperatures.[2–4] This low ductility is attributed to insufficient strain hardening due to an inability to accumulate dislocations.[4–6] For a single-phased UFG material where dislocation slip is the primary deformation mechanism, a long-standing fundamental question concerns the feasibility of developing microstructures that offer high ductility without sacrificing strength. The answer appears to be positive because there are some isolated examples where excellent mechanical behavior has been observed.[7–10] Nevertheless, the structural features contributing to high strength and good ductility remain undefined, and this lack of understanding has hindered the search for effective procedures to simultaneously improve the strength and ductility of UFG materials. Here, we report a new process in which high ductility is achieved without sacrificing strength by plastically deforming UFG Cu in liquid nitrogen. The enhanced ductility is attributed primarily to the presence of a high density of pre-existing deformation twins (PDTs) and also possibly to a large fraction of high-angle grain boundaries (HAGBs) formed during cryogenic processing. We conclude that this procedure provides a new strategy for increasing the ductility of UFG materials without any concurrent loss in strength.

Strength and ductility are often mutually exclusive, i.e., materials may be strong or ductile but are rarely both. This also applies to bulk UFG materials. The low ductility of UFG materials has invariably limited their practical application and, accordingly, much attention has been paid to the development of strategies for improving this poor ductility.[7–21] For single-phase UFG and nanostructured materials, several of the reports documenting high ductility and strength describe experiments on Cu where the stacking-fault energy is relatively low.[7,8,10–13] In some investigations the high ductility was attributed to the development of a bimodal grain size distribution[11] or pre-existing growth twins (PGTs),[12,13] but in other investigations the reasons for the high ductility were not clearly defined.[7–10] In practice, however, a bimodal grain size distribution must sacrifice some of the strength gained from nanostructuring. Another challenge is the need to fabricate UFG materials in large bulk form suitable for structural applications. This requirement has been hindered because the evidence suggests that PGTs occur only in electrodeposited thin films of nanostructured Cu,[12,13] and in nanocrystalline Cu by inert-gas condensation (IGC) followed by compaction.[22,23] However, the ductility of IGC-prepared nanocrystalline Cu is very low.[24]

The objectives of this study were twofold: First, to develop a procedure for increasing the ductility of large bulk UFG Cu without incurring any significant loss in strength. Second, to evaluate the mechanism contributing to high ductility in UFG Cu. A pure Cu (99.99 %) bar was initially processed by equal-channel angular pressing (ECAP) to produce a UFG structure (hereafter designated the UFG_{ECAP} sample), then cryodrawn (D) to a reduction in area of ca. 95 %, followed by cryorolling (R) with a reduction in thickness of ca. 96 % (hereafter designated the $UFG_{ECAP+D+R}$ sample).

Figure 1a shows that the $UFG_{ECAP+D+R}$ sample has superior mechanical properties compared to the UFG_{ECAP} sample. The UFG_{ECAP} Cu sample has a 0.2 % yield strength of ca. 410 MPa (○), which is significantly higher than the value of ca. 40 MPa in coarse-grained (CG) Cu. In addition, necking occurs rapidly after the stress reaches a maximum value, yielding a uniform elongation of only ca. 1.3 % and an elongation to failure of only ca. 5.9 % in the UFG_{ECAP} sample. By contrast, the yield strength is increased to ca. 500 MPa in the $UFG_{ECAP+D+R}$ sample, and, more importantly, this sample undergoes strain hardening, giving a uniform elongation of

[*] Dr. Y. T. Zhu, Dr. Y. H. Zhao, Dr. J. F. Bingert
Los Alamos National Laboratory
Los Alamos, NM 87545 (USA)
E-mail: yzhu@lanl.gov
Dr. X. Z. Liao
School of Aerospace, Mechanical & Mechatronic Engineering
The University of Sydney
Sydney, NSW 2006 (Australia)
Dr. B. Z. Cui, Dr. K. Han
National High Magnetic Field Laboratory
Tallahassee, FL 32310 (USA)
Dr. A. V. Sergueeva, Prof. A. K. Muhkherjee
Department of Chemical Engineering & Materials Science
University of California
Davis, CA 95616-5294 (USA)
Prof. R. Z. Valiev
Institute of Physics of Advanced Materials
Ufa State Aviation Technical University
Ufa 450000 (Russia)
Prof. T. G. Langdon
Departments of Aerospace & Mechanical Engineering
and Materials Science
University of Southern California
Los Angeles, CA 90089-1453 (USA)

[**] This project is supported by the DOE IPP program office. Supporting Information is available online from Wiley InterScience or from the author.

ADVANCED MATERIALS

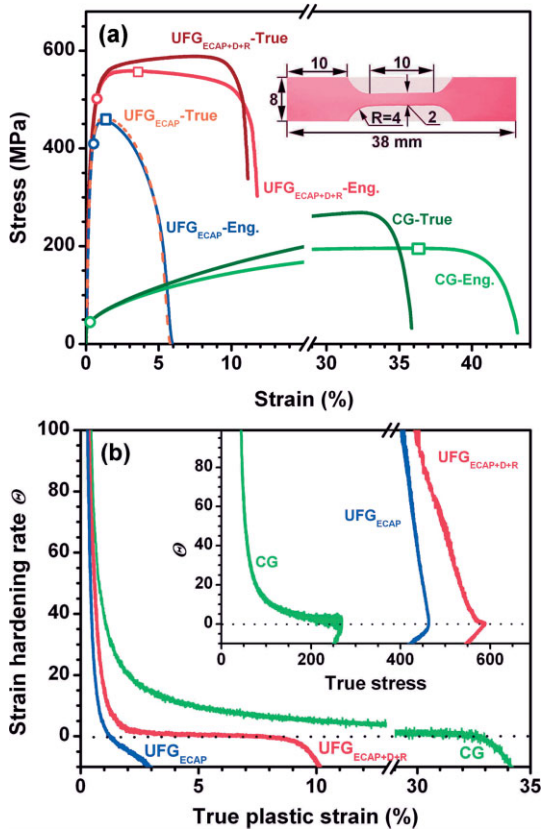

Figure 1. a) Tensile engineering and true stress–strain curves of the $UFG_{ECAP+D+R}$, UFG_{ECAP}, and coarse-grained (CG) Cu samples. □: uniform elongations, ○: 0.2 % offset yield strengths. Inset: dimensions of the tensile sample with a thickness of 0.1 mm. *R* is the radius of the arc designated by the arrow. b) Normalized strain-hardening rate (Θ) against true strain. Inset: curves of Θ against true stress.

ca. 3.5 % and a subsequent elongation to failure of ca. 11.8 %. These uniform elongations were determined using the Considère criterion,[25]

$$\left(\frac{\partial\sigma}{\partial\varepsilon}\right) \leq \sigma \qquad (1)$$

where σ is true stress and ε is true strain. The limit of uniform elongation is marked (□) on every curve. Calculations showed that the Hart criterion,[26] which includes a consideration of the strain-rate sensitivity, yields a slightly higher uniform elongation value of ca. 3.7 % for the $UFG_{ECAP+D+R}$ sample, but little difference for the UFG_{ECAP} sample. The strain-rate sensitivity (m) of the $UFG_{ECAP+D+R}$ sample was measured as $m \approx 0.018$ at a true strain of 2 %. It is important to note the large elongation occurring after the onset of necking in the $UFG_{ECAP+D+R}$ sample, which is due to the presence of continuous strain hardening as shown in the true stress–strain curve.

Figure 1b demonstrates that the $UFG_{ECAP+D+R}$ sample displays positive strain hardening to significant strains whereas, by contrast, the stress in the UFG_{ECAP} sample decreases after a small plastic strain. As shown later, this stress decrease was partially caused by strain softening. A similar strain softening was observed in many other SPD processed UFG metals and alloys.[27,28] Also, the strain-rate sensitivity of the $UFG_{ECAP+D+R}$ sample is close to the values reported for UFG Cu processed for 8–12 passes in ECAP.[8,29] Therefore, the higher ductility of the $UFG_{ECAP+D+R}$ sample is caused primarily by its higher strain-hardening rate. It is instructive to note that these experiments used tensile samples with a thickness of 0.1 mm, and work currently in progress suggests that thicker samples exhibit even higher ductilities due to a size effect (see Supporting Information, Fig. S1).

The mechanical properties of bulk solids are controlled by their microstructure. Investigations by transmission electron microscopy (TEM) indicate that the UFG_{ECAP} sample contains a large fraction of low-angle grain boundaries (LAGBs), and the subsequent cryodeformation forms numerous HAGBs and deformation twins in the $UFG_{ECAP+D+R}$ sample. Figure 2a and b shows typical bright-field TEM images of the UFG_{ECAP} and $UFG_{ECAP+D+R}$ samples, respectively. In Figure 2a, the slight contrast difference is caused by small orientation variations among the grains/subgrains. Careful examination of Figure 2a shows that most of the GBs are wavy, diffuse, and ill-defined in the UFG_{ECAP} sample, and these boundaries are primarily in a non-equilibrium state with extrinsic (non-geometrically necessary) dislocations or other interface defects.[30] The wavy and diffuse GB features are more clearly visible in high-resolution TEM images (Fig. S2). By comparison, the GBs in the $UFG_{ECAP+D+R}$ sample are sharp, clear, and relatively straight (Fig. 2b), and the contrasts between neighboring grains are larger, thereby suggesting higher misorientation angles between the adjacent grains. By tilting

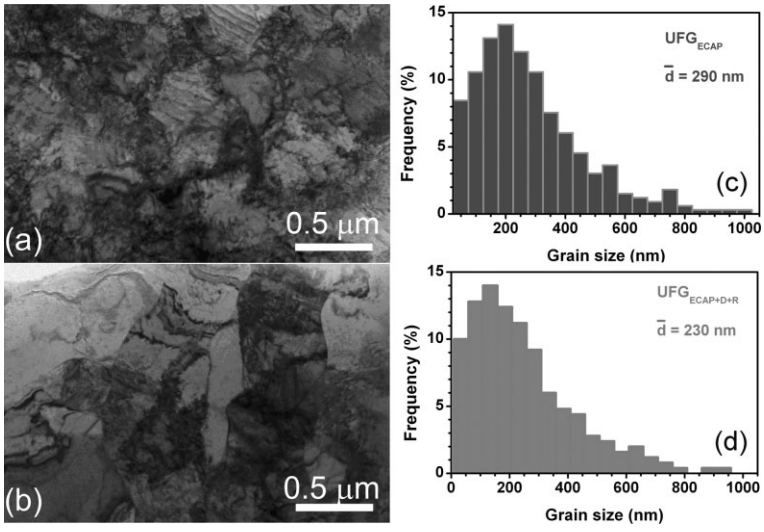

Figure 2. a,b) Typical bright-field TEM images for the UFG_{ECAP} and $UFG_{ECAP+D+R}$ Cu samples, respectively. It is apparent that the grain boundaries in the $UFG_{ECAP+D+R}$ sample are sharper and straighter than in the UFG_{ECAP} sample. c,d) Grain size distributions measured from TEM images for the UFG_{ECAP} and the $UFG_{ECAP+D+R}$ samples, where $\bar{d}$ is the average grain size.

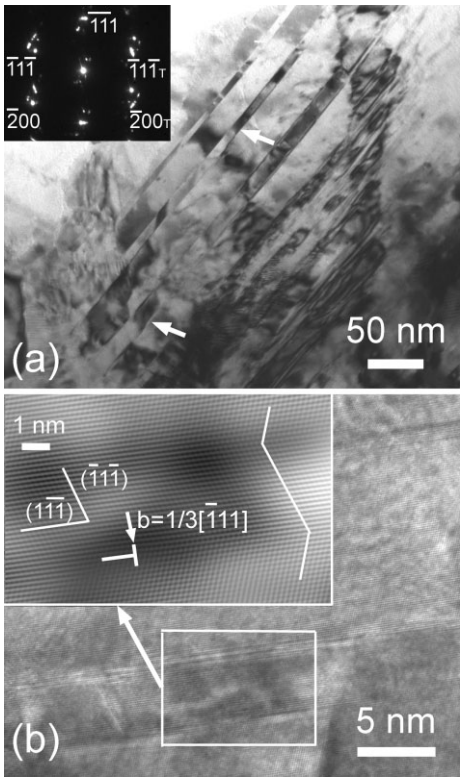

Figure 3. a) TEM image showing a grain containing a high density of PDTs in the $UFG_{ECAP+D+R}$ sample. The fading contrast of the twins on the right-hand side is due to the orientation change of the thin TEM foil. Inset: selected-area electron diffraction pattern of the twinned area. b) High-resolution TEM image taken from the <110> zone axis. Inset: twin relationship (white lines) and a Frank dislocation at a twin boundary, marked by arrow. This inset is the inverse Fourier transform (FT) of the {111} diffraction spots in the area marked by the white rectangle.

some grains to a <110> zone axis and checking the angle differences between neighboring grains/subgrains, it was found that $UFG_{ECAP+D+R}$ Cu contains a higher fraction of HAGBs than UFG_{ECAP} Cu. The grain size distributions measured from the TEM images are shown in Figure 2c and d. Both of these distributions are similar, but the average grain sizes are ca. 230 nm for $UFG_{ECAP+D+R}$ Cu and ca. 290 nm for UFG_{ECAP} Cu.

Statistical observations by TEM show that many grains in the $UFG_{ECAP+D+R}$ sample contain high densities of deformation twins, as typically shown in Figure 3a. These deformation twins have thicknesses ranging from several nanometers to ca. 85 nm and lengths in the 50–500 nm range (Fig. S3). Electron diffraction patterns of the twinned areas (inset in Fig. 3a) show that some diffraction spots are arc-shaped, indicating that the misorientations across the twin boundaries deviate slightly from 60°. Moreover, some twin boundaries are not straight (as denoted by the arrows in Fig. 3a), and this may be caused by the interactions between the twins and the dislocations during the cryodeformation.[31] High-resolution TEM revealed sessile Frank partial dislocations (Burger's vector, $b = 1/3[\bar{1}11]$, as shown in the inset of Fig. 3b by T) and glissile Shockley partials ($b = 1/6[\bar{1}\bar{2}1]$) on the twin boundaries, which may be formed by the dissociation of a full dislocation at the twin boundary through the following reaction: $1/2[\bar{1}01] \rightarrow 1/6[\bar{1}\bar{2}1] + 1/3[\bar{1}11]$.[12] By contrast, TEM revealed no evidence for any twin in the UFG_{ECAP} sample.

Quantitative electron backscatter diffraction (EBSD) analysis was used to obtain information on the distributions of the GB misorientations (Fig. 4). It is assumed that the peak occurring near 60° for $UFG_{ECAP+D+R}$ Cu is probably formed during the cryoprocessing, since it is known that low-temperature processing may introduce a large number of twin boundaries with misorientation angles of 60°.[32] In addition, the $UFG_{ECAP+D+R}$ sample has a high fraction (ca. 58 %) of HAGBs with misorientations >15°, whereas in the UFG_{ECAP} sample the fraction of HAGBs is only ca. 32 %. More specifically, for the $UFG_{ECAP+D+R}$ sample, the fraction of boundaries with misorientations in the 50°–62.8° range is ca. 23 % (which includes both deformation twins and general HAGBs), and the fraction of general HAGBs with misorientations of 15°–50° is ca. 35 %. By contrast, for the UFG_{ECAP} sample, the fractions of HAGBs in the above two ranges are ca. 9 % and ca. 24 %, respectively. These results indicate that the $UFG_{ECAP+D+R}$ sample contains larger fractions of both twin boundaries as well as general HAGBs than the UFG_{ECAP} sample, in agreement with the TEM observations. Subsequent cryorolling and the accompanying grain reorientation from the cryoprocessing in the $UFG_{ECAP+D+R}$ sample produces the observed deviation from the initial twin misorientation of 60° shown in Figure 4. Because the fundamental zone is very small for misorientations approaching the maximal value for cubic symmetry of 62.8°, the misorientation distribution becomes predominantly skewed towards lower values, as observed experimentally.

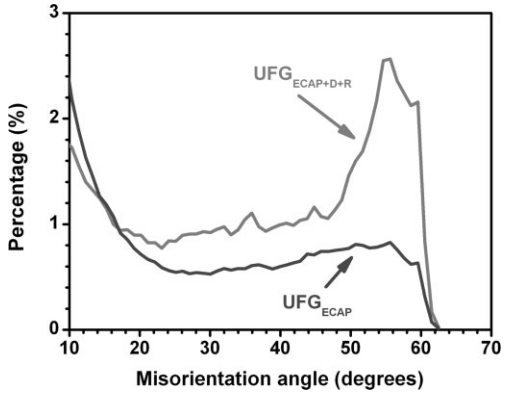

Figure 4. Distribution of grain boundary misorientation angles for the $UFG_{ECAP+D+R}$ and UFG_{ECAP} samples.

To evaluate the mechanism controlling the strain-hardening rate, the $UFG_{ECAP+D+R}$ Cu and UFG_{ECAP} Cu samples were analyzed by X-ray diffraction (XRD) before and after the ten-

ADVANCED MATERIALS

sile tests in order to measure the changes in the dislocation and twin densities (Figs. S4 and S5).[33,34] The average grain size, as measured by XRD, was ca. 50 nm for both the $UFG_{ECAP+D+R}$ and the UFG_{ECAP} samples. This value is smaller than the values measured using TEM because XRD determines the size of the coherent diffraction domains, which include the subgrains and dislocation cells.[35] It was found that tensile testing increases the dislocation density in $UFG_{ECAP+D+R}$ Cu from ca. 4.0×10^{14} to ca. 4.6×10^{14} m^{-2}, thereby suggesting that dislocation accumulation contributes to the strain hardening in the $UFG_{ECAP+D+R}$ sample. By contrast, there was a decrease in the dislocation density from ca. 4.3×10^{14} to ca. 3.0×10^{14} m^{-2} in UFG_{ECAP} Cu, suggesting that strain softening is responsible for the low ductility. The twin density, defined as the probability of finding a twin boundary between any two neighboring {111} planes, was measured as ca. 0.9 % and ca. 0.1 % before tensile testing for $UFG_{ECAP+D+R}$ and UFG_{ECAP} samples, respectively. These values were unchanged after tensile testing, showing that no twins were nucleated during the tensile testing. The twin-density value of 0.9 % was used to estimate the space between the twin boundaries as ca. 20 nm in $UFG_{ECAP+D+R}$ Cu, in qualitative agreement with the TEM observations recorded in Figure S3. Moreover, XRD patterns show the UFG_{ECAP} has a {111} texture, and cryodeformation changed this texture into a {110} rolling texture in $UFG_{ECAP+D+R}$ (Fig. S4).

The higher strength of $UFG_{ECAP+D+R}$ Cu is in part a direct consequence of the smaller grain size in comparison with UFG_{ECAP} Cu. However, it is reasonable to anticipate that the high density of twin boundaries in $UFG_{ECAP+D+R}$ Cu will act as a barrier for dislocation slip and thereby strengthen the material. In addition, the larger fraction of HAGBs in $UFG_{ECAP+D+R}$ Cu in comparison with UFG_{ECAP} Cu should be more effective in resisting dislocation slip.[36]

The experimental results suggest that the high twin density and possibly also the large fraction of HAGBs in $UFG_{ECAP+D+R}$ Cu lead to a high strain-hardening rate, and consequently a higher uniform elongation and elongation to failure. It is probable that the high density of twins plays a primary role in promoting strain hardening. Earlier reports demonstrated that PGTs are effective in blocking and storing dislocations to give an improvement in the strain-hardening rate.[13,14] In the present investigation, the twins in the $UFG_{ECAP+D+R}$ sample may be defined as PDTs because they were formed by deformation before tensile testing. These PDTs should play a similar role in improving the strain-hardening rate as the PGTs. However, it is probable that the PDTs are less effective than the PGTs because i) the increases in strength and ductility by PDTs are smaller than PGTs,[37] and ii) dislocations are already present at the boundaries of the PDTs, as shown by the high-resolution TEM image in Figure 3b. Thus, the advantage of the PDTs is their capability to be engineered into large bulk UFG Cu. It is probable that the large fraction of HAGBs in $UFG_{ECAP+D+R}$ Cu also plays a role in improving the strain-hardening rate, but most likely to a lesser extent. It is known that pure Ni subjected to cold-rolling initially has a decreasing ductility with rolling strain, such that the ductility only increases after the rolling strain has reached a certain level, probably associated with an increase in the fraction of HAGBs.[38] However, additional research is needed to evaluate the precise role of HAGBs on the strain hardening rate.

Other factors may also affect the ductility, including grain size, dislocation density, and texture, but these factors are not responsible for the high ductility observed in the $UFG_{ECAP+D+R}$ Cu. The smaller grain size in the $UFG_{ECAP+D+R}$ Cu would normally lead to a lower ductility. Also, the dislocation densities in the $UFG_{ECAP+D+R}$ and UFG_{ECAP} samples are similar, and therefore, this will have a negligible effect on the overall ductility. Furthermore, there is experimental evidence suggesting that the {110} rolling texture in the $UFG_{ECAP+D+R}$ Cu should lead to a lower ductility compared to UFG_{ECAP} Cu.[39]

In summary, this study demonstrates the occurrence of simultaneous improvements in the ductility and strength of UFG materials by introducing PDTs and increasing the fraction of HAGBs. This study also presents a processing strategy designed to improve the ductility of UFG materials without any loss of strength. Experiments on high-purity Cu show that this strategy can be successfully used to produce bulk UFG materials having the high strength and good ductility required for use in practical structural applications. Although the specimens in the present study are relatively small, the strategy developed here can be readily scaled up to process large bulk UFG materials for practical applications.

Experimental

A high-purity (99.99 %) Cu bar with a diameter of 20 mm was processed at room temperature by ECAP for 12 passes, using a die with an internal channel angle of 90° and processing route B_C (rotating the sample by 90° clockwise after each pass). The ECAP-processed Cu bar was cryogenically extruded at 77 K to form a UFG Cu wire with a diameter of 4.5 mm. Both the wire and dies were immersed in liquid nitrogen to ensure that cryogenic drawing was performed at 77 K. The UFG wire was then cryogenically rolled to a thickness of 0.2 mm. The total thickness reduction was 95.6 % after multiple rolling passes, with a thickness reduction of approximately 10 % in each pass (Fig. S6).

For tensile testing, the samples were cut into dog-bone-shaped specimens with a gauge length of 10 mm and a width of 2 mm, and polished to a thickness of 0.1 mm. Uniaxial tensile tests were performed at room temperature using a Shimazu Universal Tester with an initial quasi-static strain rate of 1.7×10^{-4} s^{-1}. Five specimens were used for each condition to obtain consistent stress–strain curves.

XRD measurements were conducted using a Scintag X-ray diffractometer operating at 1.8 kW and equipped with a Cu target. The gauge sections of the tensile specimens were examined using XRD before and after tensile testing to determine the change in the dislocation and twin densities (Fig. S7). The errors in the XRD-measured dislocation densities were estimated as less than 10 %. TEM measurements were performed using an FEI Tecnai F30 microscope operating at 300 kV. Specimens for TEM were prepared by mechanically grinding the samples to a thickness of about 10 μm, and then thinned further to a thickness of electron transparency using a Gatan Dual Ion Milling system with an Ar^+ accelerating voltage of 4 kV, and liq-

uid nitrogen to cool the specimen. The EBSD samples were first polished using a diamond lapping film (particle diameter 1 μm) and then electropolished in a solution of 66 % H_3PO_4 and 34 % H_2O at 2 V. EBSD scans were performed using a TSL OIM system on a Philips XL30 FEG TEM apparatus with step sizes of 100 or 130 nm.

Received: July 2, 2006
Revised: August 12, 2006
Published online: October 27, 2006

[1] R. Z. Valiev, Y. Estrin, Z. Horita, T. G. Langdon, M. J. Zehetbauer, Y. T. Zhu, *JOM* **2006**, *58*, 33.
[2] C. C. Koch, *Scr. Mater.* **2003**, *49*, 657.
[3] D. Jia, Y. M. Wang, K. T. Ramesh, E. Ma, Y. T. Zhu, R. Z. Valiev, *Appl. Phys. Lett.* **2001**, *79*, 611.
[4] Y. T. Zhu, X. Z. Liao, *Nat. Mater.* **2004**, *3*, 351.
[5] H. van Swygenhoven, J. R. Weertman, *Scr. Mater.* **2003**, *49*, 625.
[6] Z. Budrovic, H. van Swygenhoven, P. M. Derlet, S. V. Petegem, B. Schmitt, *Science* **2004**, *304*, 273.
[7] R. Z. Valiev, I. V. Alexandrov, Y. T. Zhu, T. C. Lowe, *J. Mater. Res.* **2002**, *17*, 5.
[8] Y. M. Wang, E. Ma, M. W. Chen, *Appl. Phys. Lett.* **2002**, *80*, 2395.
[9] H. W. Höppel, J. May, M. Göken, *Adv. Eng. Mater.* **2004**, *6*, 781.
[10] K. M. Youssef, R. O. Scattergood, K. L. Murty, J. A. Horton, C. C. Koch, *Appl. Phys. Lett.* **2005**, *87*, 091 904.
[11] Y. Wang, M. Chen, F. Zhou, E. Ma, *Nature* **2002**, *419*, 912.
[12] L. Lu, Y. Shen, X. Chen, L. Qian, K. Lu, *Science* **2004**, *304*, 422.
[13] E. Ma, Y. M. Wang, Q. H. Lu, M. L. Sui, L. Lu, K. Lu, *Appl. Phys. Lett.* **2004**, *85*, 4932.
[14] B. Q. Han, Z. Lee, D. Witkin, S. Nutt, E. J. Lavernia, *Metall. Mater. Trans. A* **2005**, *36*, 957.
[15] Y. B. Lee, D. H. Shin, K. T. Park, W. J. Nam, *Scr. Mater.* **2004**, *51*, 355.
[16] Z. Horita, K. Ohashi, T. Fujita, K. Kaneko, T. G. Langdon, *Adv. Mater.* **2005**, *17*, 1599.
[17] J. K. Kim, H. K. Kim, J. W. Park, W. J. Kim, *Scr. Mater.* **2005**, *53*, 1207.
[18] H. W. Kim, S. B. Kang, N. Tsuji, Y. Minamino, *Acta Mater.* **2005**, *53*, 1737.
[19] Y. H. Zhao, X. Z. Liao, S. Cheng, E. Ma, Y. T. Zhu, *Adv. Mater.* **2006**, *18*, 2280.
[20] Y. H. Zhao, Y. T. Zhu, X. Z. Liao, Z. Horita, T. G. Langdon, *Appl. Phys. Lett.* **2006**, *89*, 121 906.
[21] E. Ma, *JOM* **2006**, *58*, 49.
[22] G. W. Nieman, J. R. Weertman, R. W. Siegel, *Mat. Res. Soc. Symp. Proc.* **1991**, *206*, 493.
[23] P. G. Saners, A. B. Witney, J. R. Weertman, R. Z. Valiev, R. W. Siegel, *Mater. Sci. Eng. A* **1995**, *204*, 7.
[24] G. W. Nieman, J. R. Weertman, R. W. Siegel, *J. Mater. Res.* **1991**, *6*, 1012.
[25] G. E. Dieter, *Mechanical Metallurgy*, 3rd ed., McGraw-Hill, New York **1986**, 289.
[26] E. W. Hart, *Acta Metall.* **1967**, *15*, 351.
[27] Z. Horita, T. Fujinami, M. Nemoto, T. G. Langdon, *Metall. Mater. Trans. A* **2000**, *31*, 691.
[28] T. R. Lee, C. P. Chang, P. W. Kao, *Mater. Sci. Eng. A* **2005**, *408*, 131.
[29] F. H. Dalla Torre, E. V. Pereloma, C. H. J. Davies, *Scr. Mater.* **2004**, *51*, 367.
[30] J. Y. Huang, Y. T. Zhu, H. G. Jiang, T. C. Lowe, *Acta Mater.* **2001**, *49*, 1497.
[31] J. W. Christian, S. Mahajan, *Prog. Mater. Sci.* **1995**, *39*, 1.
[32] K. Han, R. P. Walsh, A. Ishmaku, V. Toplosky, J. D. Embury, *Philos. Mag.* **2004**, *84*, 3705.
[33] Y. H. Zhao, H. W. Sheng, K. Lu, *Acta Mater.* **2001**, *49*, 365.
[34] J. B. Cohen, C. N. J. Wagner, *J. Appl. Phys.* **1962**, *33*, 2073.
[35] Y. T. Zhu, J. Y. Huang, J. Gubicza, T. Ungár, Y. M. Wang, E. Ma, R. Z. Valiev, *J. Mater. Res.* **2003**, *18*, 1908.
[36] B. Chalmers, *Proc. R. Soc. London A* **1937**, *162*, 120.
[37] Y. F. Shen, L. Lu, Q. H. Lu, Z. H. Jin, K. Lu, *Scr. Mater.* **2005**, *52*, 989.
[38] S. S. Hecker, M. G. Stout, in *Deformation, Processing and Structure* (Ed: G. Krauss), ASM Int., Materials Park, OH **1984**.
[39] F. Ebrahimi, Q. Zhai, D. Kong, *Scr. Mater.* **1998**, *39*, 315.

